A parallel mechanism of the shoulder - application to multi-body optimisation

Aimad El Habachi, Sonia Duprey, Laurence Cheze, Raphaël Dumas

Multibody System Dynamics

April 2015, Volume 33, Issue 4, pp 439-451

A parallel mechanism of the shoulder – application to multi-body optimisation

Aimad El Habachi, Sonia Duprey, Laurence Cheze and Raphaël Dumas

Corresponding author: raphael.dumas@ifsttar.fr

Université de Lyon, F-69622, France

IFSTTAR, LBMC, UMR_T9406, Bron

Université Lyon 1, Villeurbanne, France

Abstract:

This paper describes and evaluates a parallel mechanism of the shoulder girdle. This mechanism was a closed kinematic chain composed of three segments (humerus, scapula and thorax) and three kinematic constraints. The clavicle was modelled as a constant length constraint between the sternoclavicular and acromioclavicular joint centres. The second kinematic constraint was also a constant length between the glenoid cavity and the humeral head for the glenohumeral joint. The third constraint was a point-on-ellipsoid contact for the scapulothoracic joint. Geometrical data required to build this kinematic model were obtained from the Visible Human Project.

The parallel mechanism was then introduced into a multi-body optimisation for the computation of the scapulothoracic joint angles from surface sensors during the abduction of the arm of six able-bodied subjects. The initial guess of this optimisation was obtained by an acromial method. Compared to palpation of scapula anatomical landmarks, the multi-body optimisation with the proposed parallel mechanism allows estimating the shoulder kinematics with a better accuracy than the acromial method alone.

Keywords: Shoulder girdle, Acromial method, Palpation, Kinematic constraints, Scapulothoracic joint angles.

Introduction

Injuries related to shoulder dynamic movements were increasingly common, affecting people due to sport activities, restrained or repetitive working postures, etc. Additionally, shoulder kinematics was very complex since the movement of the scapula was constrained by the thorax, clavicle and humerus motions.

Non-invasive dynamic measurement methods based on skin markers or surface sensors were commonly used to evaluate shoulder kinematics. The anatomical landmarks, segment coordinate systems and joint coordinate systems have been standardized by the International Society of Biomechanics (ISB) [1]. However, the measurement methods based on skin markers or surface sensors have a limited accuracy due to the relative movement between the skin and the underlying bones. These soft tissue artefacts were especially important for the scapula [2-4]. Therefore, compensations of the soft tissue artefacts for the shoulder have been proposed, such as multi-body optimisation [5-10].

Multi-body optimisations rely on the minimisation of distances between the skin markers and the model-determined markers positions. The shoulder complex was usually modelled with an open kinematic chain: clavicle, scapula and humerus linked with spherical sternoclavicular, acromioclavicular and glenohumeral joints [11-13]. However, describing upper limb kinematics as an open chain was not realistic, since physiologically, the scapula was posteriorly related to the thorax by a scapulothoracic contact.

The objective of this paper was to describe a parallel mechanism of the shoulder girdle within a closed kinematic chain for application in a multi-body optimisation framework. The parallel mechanism was made of three kinematic constraints between the scapula, the thorax and the humerus. The clavicle was not explicitly introduced as a segment but was considered as one of the kinematic constraints: a constant length between the sternoclavicular and acromioclavicular joint centres. A second kinematic constraint was introduced to model the scapulothoracic joint. This was a point-on-ellipsoid contact (where the contact point belongs to the scapula and the ribcage was modelled with an ellipsoid). Another constant length constraint between the glenoid centre and the humeral head was considered for the glenohumeral joint. The geometrical data defining these joints were taken from the Visible Human Project (VHP) [14].

The parallel mechanism of the shoulder was introduced into a multi-body optimisation framework [15]. The multi-body optimisation was applied to the upper limb movements of six able-bodied subjects and the kinematics of the scapula were compared to those obtained from a palpation method. The initial guess of this optimisation was obtained using an acromial method [16-20].

Kinematic data

Six able-bodied and right-handed male subjects (age: 22.67±1.97, BMI: 22.12±2.10 kg/m²) gave their informed consent to participate in the study. Using the 3D Guidance trackSTAR 2™ (©2010 Ascension Technology Corporation. P.O. Box 527 Burlington, VT 05402), a physiotherapist placed three surface sensors on the superior part of the arm at the level of the deltoid tuberosity of the humerus, on the flat surface of acromion and on the back at the level of 1st thoracic vertebra of the subject in a standing static posture (Figure 1a). These three sensors were used to obtain the six degrees of freedom of the segment on which they were pasted during the analysed movement. A fourth sensor was used as palpator to locate the anatomical landmarks of the upper limb and thorax in the static posture: incisura jugularis (IJ), processus xiphoideus (PX) and 8th thoracic vertebra (T8), 7th cervical vertebra (C7) for the thorax segment; acromioclcavicular (AC), trigonum spinae (TS), angulus acromialis (AA), and angulus inferior (AI) for the scapula segment; lateral humeral epicondyle (LE) and medial humeral epicondyle (ME) for the humerus segment [1]. After the calibration process, the subject was asked to lay on his stomach and to remain relaxed on a table inclined at an angle of 30° (Figure 1b). This angle of inclination was chosen so that the arm abduction was in the scapular plane. The physiotherapist moves the subject's arm achieving sequential abduction movement at 0°, 45°, 90°, 120°, 140° and 160°. At each arm abduction angle, the physiotherapist palpated the anatomical landmarks of the scapula (AA, TS and AI) (Figure 1-b). This protocol was the same as in other studies using the acromial method compared to palpation method [3, 17, 20-22]. Typically, in the acromial method [16-20], the pose of the scapula was obtained through the transformation provided by the surface sensor fixed on the acromion, from the static posture to the other postures during the arm movement. In the palpation method, the pose of the scapula was obtained through a least square matching [23] of the AA, TS and AI positions, palpated in the static and other postures.

Geometrical data

This study was based on the VHP data described in [24]. This database contained all the landmarks for thorax segment (C7, IJ, T8, PX) and scapula segment (AA, TS, AI). For the joints, the AC and sternoclavicular joint centre (SC), the ellipsoid centre (EC), ellipsoid orientation and radii, as well as the two contact points (IM and SM) located on the inner surface of the scapula for the scapula-thoracic joint were also derived from this database. In this study, only one contact point (P) was considered and was located at mid-distance between these two contact points.

Since the landmarks palpated on the subjects were external whilst the corresponding landmarks provided by [24] were internal (i.e., bony landmarks), the VHP data [14] was completed by adding virtual external landmarks (see appendix). The external landmarks digitized on VHP were C7, IJ, T8 and PX on the thorax, AA, TS and AI on the scapula. Moreover, the glenoid cavity (GC) and the humeral head (HH) centres and radii were estimated using a least square method.

The VHP geometry was different from the subjects' geometry and was then transformed using affine approximation [25, 26] based on the external landmarks C7, IJ, T8, PX, AA, AC, TS and AI in the standing static posture (Figure 2a). The coefficients of this affine approximation were determined using a least square method. The homothethy and rotation transformations were extracted from the affine approximation [25] and applied to the radii and axes of the ellipsoid.

Multi-body optimisation

Constrained minimisation

The optimisation problem was:

$$\min_{\mathbf{Q}} f = \frac{1}{2}\left(\mathbf{\Phi}^m\right)^T \mathbf{\Phi}^m$$
$$\text{subject to } \begin{cases} \mathbf{\Phi}^k \\ \mathbf{\Phi}^r \end{cases}, \tag{1}$$

with $\mathbf{Q} = \begin{bmatrix} \mathbf{Q}_1 \\ \mathbf{Q}_2 \\ \mathbf{Q}_3 \end{bmatrix}$ the segment parameters to be optimised with i = 1, 2, 3 for the humerus, scapula and thorax segments respectively, $\mathbf{\Phi}^m$ the motor constraints involved in the objective function f, $\mathbf{\Phi}^k = \begin{bmatrix} \Phi^k_{GH} \\ \Phi^k_{C} \\ \Phi^k_{ST} \end{bmatrix}$ the kinematic constraints with *GH*, *C* and *ST* respectively for the glenohumeral, clavicle (i.e., sternoclavicular and acromioclavicular) and scapulothoracic joints, and $\mathbf{\Phi}^r = \begin{bmatrix} \mathbf{\Phi}^r_1 \\ \mathbf{\Phi}^r_2 \\ \mathbf{\Phi}^r_3 \end{bmatrix}$ the rigid body constraints.

The optimisation problem was equivalent to a zero-search problem:

$$\mathbf{F}\begin{pmatrix} \mathbf{Q} \\ \boldsymbol{\lambda}^k \\ \boldsymbol{\lambda}^r \end{pmatrix} = \begin{bmatrix} \left[\mathbf{K}^m\right]^T \mathbf{\Phi}^m + \begin{bmatrix} \mathbf{K}^k & \mathbf{0} \\ \mathbf{0} & \mathbf{K}^r \end{bmatrix}^T \begin{pmatrix} \boldsymbol{\lambda}^k \\ \boldsymbol{\lambda}^r \end{pmatrix} \\ \begin{pmatrix} \mathbf{\Phi}^k \\ \mathbf{\Phi}^r \end{pmatrix} \end{bmatrix} = \mathbf{0}\ , \tag{2}$$

with $\mathbf{K}^m$ the Jacobian matrix of the motor constraints, $\boldsymbol{\lambda}^k$, $\boldsymbol{\lambda}^r$ and $\mathbf{K}^k$, $\mathbf{K}^r$ the Langrange multipliers and Jacobian matrices of the kinematic constraints and rigid body constraints.

The Jacobian matrices were derived analytically and the zero-search problem was solved with *fsolve* Matlab function.

Segment parameters

The generalised coordinates $\mathbf{Q}_i = \begin{bmatrix} \mathbf{u}_i \\ \mathbf{r}_{P_i} \\ \mathbf{r}_{D_i} \\ \mathbf{w}_i \end{bmatrix}$ [15, 27] were used to describe the pose of the segments. They were a typical set of natural coordinates [28] with two position and two orientation vectors expressed in an inertial coordinate system (ICS). In the static position, the parameters $\mathbf{Q}_i$ were constructed using the procedure listed below (Figures 2a & b):

- $\mathbf{Q}_1$ of the humerus segment:
  - ✓ $\mathbf{r}_{P_1}$ was the position of HH (transformed from VHP data using the affine approximation)
  - ✓ $\mathbf{r}_{D_1}$ was the position of the midpoint between LE and ME
  - ✓ $\mathbf{w}_1$ was the unitary vector from ME to LE
  - ✓ $\mathbf{u}_1$ was perpendicular to $\mathbf{v}_1 = \mathbf{r}_{P_1} - \mathbf{r}_{D_1}$ and $\mathbf{w}_1$, unitary, and points anteriorly
- $\mathbf{Q}_2$ of the scapula segment:
  - ✓ $\mathbf{r}_{P_2}$ was the position of the internal AC (transformed from VHP data using the affine approximation)
  - ✓ $\mathbf{r}_{D_2}$ was the position of GC (transformed from VHP data using the affine approximation)
  - ✓ $\mathbf{w}_2$ was the unitary vector from the internal landmarks AA to TS (transformed from VHP data using the affine approximation).
  - ✓ $\mathbf{u}_2$ was the normal vector to the scapular plane (formed by internal landmarks AA, TS and AI transformed from VHP data using the affine approximation), unitary, and points anteriorly
- $\mathbf{Q}_3$ of the thorax segment:

- ✓ $\mathbf{r}_{P_3}$ was the position of the midpoint between the external IJ and C7
- ✓ $\mathbf{r}_{D_3}$ was the position of the midpoint between external PX and T8
- ✓ $\mathbf{w}_3$ was perpendicular to $\mathbf{v}_3 = \mathbf{r}_{P_3} - \mathbf{r}_{D_3}$ and the vector formed by mid-points of C7 and IJ and the mid-points of PX and IJ, unitary, and points to the right
- ✓ $\mathbf{u}_3$ was perpendicular to $\mathbf{v}_3 = \mathbf{r}_{P_3} - \mathbf{r}_{D_3}$ and $\mathbf{w}_3$, unitary, and points anteriorly

The geometrical parameters (e.g., segment lengths $L_i = \left\| \mathbf{r}_{P_i} - \mathbf{r}_{D_i} \right\|$) were also determined in the subject's standing static posture. The initial values of $\mathbf{Q}_i$ used in optimisation were constructed using the transformation provided by the sensors from the static position to the other positions during the arm movement. In other words, the principle of the acromial method, that was to say a CAST-like method [29, 30], was used for all segments. Moreover, in order to keep the classical objective function of the multi-body optimisation (i.e., distance between measured and model-determined skin marker positions [15]) the position of the anatomical landmarks (C7, IJ, T8, PX, AC, AA, ME, and LE) were also transformed from the static to the other postures using the same transformations.

Motor constraints

The objective function *f* was described as in the squared distance between measured and model-determined external anatomical landmarks [15]. The anatomical landmarks used were: C7, IJ, T8, PX, AC, AA, AI, LE, and ME (Figure 2a).

The motor constraints were:

$$\mathbf{\Phi}^m = \left\{ \begin{array}{c} \vdots \\ \mathbf{r}_{M_i^j} - \mathbf{N}_i^{M_i^j} \mathbf{Q}_i = \mathbf{0}, \\ \vdots \end{array} \right. \quad (3)$$

with $r_{M_i^j}$ the position and $\mathbf{N}_i^{M_i^j}$ the interpolation matrix [27, 28] for one anatomical landmark (i.e., denoted j^{th} external (or marker) landmarks of the i^{th} segment).

Kinematic constraints

As previously explained, the kinematic constraint of the glenohumeral joint was that the distance between the HH and GC centres remains unchanged during the movement (Figure 2b). This constraint was (4):

$$\Phi_{GH}^k = \left(\mathbf{r}_{P_1} - \mathbf{r}_{D_2}\right)^2 - d_1^2 = 0 . \quad (4)$$

The distance d_1 was the distance between HH and GC centres transformed from VHP data using the affine approximation.

The clavicle was not introduced in the kinematic model as a segment in order to reduce the number of variables during the optimisation phase. It was considered as a kinematic constraint by keeping the distance between the acromioclavicular and sternoclavicular joint centres unchanged during the movement (Figure 2). This constraint was:

$$\Phi_C^k = \left(\mathbf{r}_{P_2} - \mathbf{N}_3^{V_3^1}\mathbf{Q}_3\right)^2 - d_2^2 = 0 , \quad (5)$$

where $\mathbf{N}_3^{V_3^1}$ was the interpolation matrix for the SC joint centre (i.e., 1^{rst} internal (virtual) landmark of segment 3). The distance d_2 was the clavicle length (transformed from VHP data using the affine approximation).

The scapulothoracic joint was modelled as a unique point of the scapula in contact with the ellipsoid of the ribcage [7]. This constraint was:

$$\Phi_{ST}^k = (\mathbf{N}_2^{V_2^1}\mathbf{Q}_2 - \mathbf{N}_3^{V_3^2}\mathbf{Q}_3)^T \mathbf{R}\mathbf{A}\mathbf{R}^T (\mathbf{N}_2^{V_2^1}\mathbf{Q}_2 - \mathbf{N}_3^{V_3^2}\mathbf{Q}_3) - 1 = 0 , \quad (6)$$

with $\mathbf{N}_3^{V_3^2}$ the interpolation matrix for EC (i.e., 2[d] internal (virtual) landmark of segment 3), $\mathbf{N}_2^{V_2^1}$ the interpolation matrix for P (i.e., 1[rst] internal (virtual) landmark of segment 2), $\mathbf{A} = \begin{bmatrix} \frac{1}{a^2} & 0 & 0 \\ 0 & \frac{1}{b^2} & 0 \\ 0 & 0 & \frac{1}{c^2} \end{bmatrix}$ the matrix with *a*, *b* and *c* the radial ellipsoid dimensions (transformed from VHP data using the affine approximation). **R** was the rotation matrix from the ICS (inertial coordinate system) to the ellipsoid coordinate system. This rotation matrix can be computed as shown below:

$$\mathbf{R} = \left[\mathbf{u}_3 \quad \mathbf{r}_{P_3} - \mathbf{r}_{D_3} \quad \mathbf{w}_3\right]\left(\mathbf{B}_3^{\mathbf{u}}\right)^{-1}\mathbf{C}\,, \tag{7}$$

$$\text{with } \mathbf{B}_3^{\mathbf{u}} = \begin{pmatrix} 1 & L_3\cos\gamma_3 & \cos\beta_3 \\ 0 & L_3\sin\gamma_3 & \dfrac{\cos\alpha_3 - \cos\beta_3\cos\gamma_3}{\sin\gamma_3} \\ 0 & 0 & \sqrt{\sin^2\beta_3 - \left(\dfrac{\cos\alpha_3 - \cos\beta_3\cos\gamma_3}{\sin\gamma_3}\right)^2} \end{pmatrix}.$$

Matrix $\mathbf{B}_3^{\mathbf{u}}$ was the constant rotation from the axes $\mathbf{u}_3$, $\mathbf{r}_{P_3} - \mathbf{r}_{D_3}$ and $\mathbf{w}_3$ to the thorax segment coordinate system (SCS) [27]. L_3 was the segment length, α_3, β_3 and, γ_3 were the angles between $(\mathbf{u}_3, \mathbf{r}_{P_3} - \mathbf{r}_{D_3})$, $(\mathbf{r}_{P_3} - \mathbf{r}_{D_3}, \mathbf{w}_3)$ and $(\mathbf{w}_3, \mathbf{u}_3)$ respectively [27] and therefore, matrix $\mathbf{B}_3^{\mathbf{u}}$ was constant and non-singular by construction. Matrix **C** was the rotation from the thorax SCS to the ellipsoid coordinate system (transformed from VHP data using the affine approximation).

Rigid body constraints

The rigid body constraints for each segment *i* was [15, 27]:

$$\mathbf{\Phi}_i^r = \begin{cases} \mathbf{u}_i{}^2 - 1 = 0 \\ \mathbf{u}_i \bullet \left(\mathbf{r}_{P_i} - \mathbf{r}_{D_i} \right) - L_i \cos\gamma_i = 0 \\ \mathbf{u}_i \bullet \mathbf{w}_i - \cos\beta_i = 0 \\ \left(\mathbf{r}_{P_i} - \mathbf{r}_{D_i} \right)^2 - L_i{}^2 = 0 \\ \left(\mathbf{r}_{P_i} - \mathbf{r}_{D_i} \right) \bullet \mathbf{w}_i - L_i \cos\alpha_i = 0 \\ \mathbf{w}_i{}^2 - 1 = 0 \end{cases} . \quad (8)$$

Joint angles comparison

The angles of the scapulothoracic joint were computed following the ISB standardisation [1], using a $\mathbf{Y}_2$, $\mathbf{X}_f$, $\mathbf{Z}_3$ sequence: internal(+)/external(-) rotation, downward(+)/upward(-) rotation and posterior(+)/anterior(-) tilt. The angles of the glenohumeral joint were computed following the recommendation of [31]. For the abduction movement of the arm, the sequence was $\mathbf{X}_2$, $\mathbf{Z}_f$, $\mathbf{Y}_3$: adduction(+)/abduction(-), flexion(+)/extension(-), internal(+)/external(-) rotation. These angles can be computed directly from $\mathbf{Q}_i$ [32], using the previously defined matrix $\mathbf{B}$. The angles obtained with the initial values (i.e., acromial method), with the optimised values and with the reference values (i.e., palpation method) were compared. Only the scapulothoracic joint angles were presented in the next section. For comparison purposes, the axes of the scapula obtained by the acromion method, the multi-body optimisation and the palpation method have been aligned in the lying posture at 0° of arm abduction. Then, the root mean square error (RMSE) of the acromial method and multi-body optimisation vs. palpation method at each arm abduction angle was computed and the differences between the means were tested using a t-test.

Results

The optimisation was achieved in less than five seconds for each arm abduction position. The scapulothoracic joint angles obtained by the acromial method, this optimisation, and the palpation method were displayed in Figure 3. The scapula rotates internally and upwardly and tilts posteriorly during the abduction movement of the arm (Figure 3), with large inter-subject variabilities. The results obtained using the acromial method and the multi-body optimisation show the same tendency as those obtained from the palpation method.

Table 1 gives the mean and the standard deviation of the RMSE calculated on all the arm abductions. As shown in this table, the multi-body optimisation improves the downward/upward rotation and the posterior/anterior tilt compared to the acromial method. However, it deteriorates slightly the internal/external rotation. The acromial method was overestimating this rotation while the multi-body optimisation was underestimating it. However, the t-test indicates that the difference between means obtained using the multi-body optimisation and palpation method was not significant for any of the arm abduction and scapulothoracic joint angles. On the other hand, the difference between means obtained between acromial and palpation methods was significant for the downward/upward rotation at 45° and 90° as well as for the posterior/anterior tilt at 90°, 120°, 140° and 160°.

Discussion

The aim of this paper was to propose a parallel mechanism of the shoulder based on scaled VHP geometrical data. This kinematic model was a closed chain consisting of thorax, scapula and humerus. The clavicle was not considered as a segment. It was one of the two kinematic constraints between the thorax and the scapula. The other kinematic constraints of the model can be described as two contacts: a sphere-on-sphere contact between the glenoid and the

humeral head and a point-on-ellipsoid contact between the scapula and the ribcage. In the proposed parallel mechanism, the number of degrees of freedom of the shoulder girdle (i.e., considering the thorax fixed) was nine. It was higher than other models of the literature [11-13], except for a model with spherical sternoclavicular, acromioclavicular and glenohumeral joints that was an open chain. These kinematic models have been widely used in the literature for multi-body optimisation and musculoskeletal modelling [5-9, 33, 34]. In all these studies, the glenohumeral joint was always spherical, thus not allowing for any displacement. The introduction of a sphere-on-sphere contact, through a simple constant length constraint, may be considered as more physiologically accurate. Moreover, in most multi-body optimisations, the shoulder girdle was an open chain [6, 8, 9] and the movement of the scapula was not considered. The parallel mechanism proposed in this study was a closed chain with one point-on-ellipsoid contact as proposed by [7]. Models with two contact points have been more commonly used [5, 33, 34], but there was no general consensus on this choice and the proposed parallel mechanism could be easily adapted using equation 3 twice with two different points (i.e., IM and SM, see appendix). The multi-body optimisation framework used in this study [15] was previously developed to be able to easily introduce different sets of kinematic constraints and therefore, comparisons such as using one or two point-on-ellipsoid contacts, or leaving one of the three kinematic constraints out can be performed in future studies. Moreover, it can be noted that in the multi-body optimisation framework, the objective function and the constraints were all quadratic, except one of 4^{th} order, and that the solution domain was unbounded. This was a consequence of using the generalised coordinates $\mathbf{Q}_i$ [15] that were fully Cartesian coordinates [28].

The multi-body optimisation was performed for the computation of the scapulothoracic joint angles and glenohumeral joint displacements from external landmarks during abduction of the arm up to 160°. The results were consistent with the literature [16, 35-39] where the shoulder

movements were measured using intra-cortical pins or fluoroscopy. The results of the multi-body optimisation were also compared to palpation. The acromial method was used to obtain the initial guess. The multi-body optimisation seems to improve the downward/upward rotation and posterior/anterior tilt but not the internal/external rotation, which was found to be slightly deteriorated during arm abduction. The improvement of downward/upward rotation and posterior/anterior tilt was confirmed by the significant differences of means between acromial method and palpation method but not between multi-body optimisation and palpation method. For the internal/external rotation, underestimated with the acromial method and overestimated with the multi-body optimisation, the differences of means were, still, non-significant. Some inconsistencies may be attributed to the point-on-ellipsoid constraint between the scapula and the ribcage. It could be anticipated that introducing two contact points would have been even worse because, physiologically, the contact point(s) cannot remain fixed in the scapula. In this way, the proposed parallel mechanism of the shoulder could be further improved using a plane-on-ellipsoid contact. In all cases, the introduction of kinematic constraints seems to be more appropriate than the introduction of couplings between the degrees of freedom, such as the scapulo-humeral rhythm [40, 41]. A recent study [42] demonstrated that kinematic constraints were necessary to be added to this rhythm in order to obtain physiologically-acceptable shoulder kinematics.

This study presents several limits. Firstly, the proposed parallel mechanism was based on VHP geometrical data, adapted but not subject-specific. In future studies, the geometrical parameters of the joints may be personalised using medical imaging. The subject-specificity was considered as crucial because a sensitivity analysis revealed that the scapula kinematics was highly influenced by the geometrical parameter of the parallel mechanism and specifically, the length of the clavicle [43]. Indeed, as shown in table 1, the parallel mechanism restrains the movement due to the imposed kinematic constraints and reduces the

inter-subjects variability. In a personalisation perspective, the modification of the geometrical parameters (e.g., length of the clavicle, position and size of thorax ellipsoid) from medical imaging appears simpler than the modification of scapulohumeral rhythm [40, 41]. Second, the multi-body optimisation was performed on six subjects and compared to palpation that was a silver standard prone to error [44]. However, particular attention was paid to the palpation protocol (i.e., scapular plane, relaxed subject) and for instance, the RMSE between the acromial and palpation methods were in the lower bound of the literature [3, 17, 20-22], especially in the extreme positions of the arm in abduction. The method should now be validated against a gold standard (i.e., intra-cortical pins or fluoroscopy).

This study demonstrated that a multi-body optimisation using the proposed parallel mechanism allows the estimation of the scapular motion accurately when compared to palpation. This method uses the acromial method as initial guess and improves the scapulothoracic kinematics except, to some extent, the internal/external rotation.

Acknowledgement

This study was supported by the "Agence Nationale pour la Recherche" and the "Pôle de Compétitivité Sporaltec" [ANR ACE n°2010-BLANC-901].

The authors wish to thank Mr Samuel Barbaste from the LBMC UMR_T9406 for his help during experimentation.

Reference:

1. Wu, G., et al., *ISB recommendation on definitions of joint coordinate systems of various joints for the reporting of human joint motion—Part II: shoulder, elbow, wrist and hand.* J Biomech, 2005. **38**(5): p. 981-992.
2. Matsui, K., K. Shimada, and P.D. Andrew, *Deviation of skin marker from bone target during movement of the scapula.* J Orthop Sci, 2006. **11**(2): p. 180-4.
3. Lempereur, M., et al., *Difference between palpation and optoelectronics recording of scapular motion.* Comput Methods Biomech Biomed Engin, 2010. **13**(1): p. 49-57.
4. Bourne, D.A., et al., *A new subject-specific skin correction factor for three-dimensional kinematic analysis of the scapula.* J Biomech Eng, 2009. **131**(12): p. 121009.
5. Ausejo, S., Á. Suescun, and J. Celigüeta, *An optimization method for overdetermined kinematic problems formulated with natural coordinates.* Multibody System Dynamics, 2011. **26**(4): p. 397-410.
6. Jackson, M., et al., *Improvements in measuring shoulder joint kinematics.* J Biomech, 2012. **45**(12): p. 2180-3.
7. Maurel, W. and D. Thalmann, *Human shoulder modeling including scapulo-thoracic constraint and joint sinus cones.* Computers & Graphics, 2000. **24**(2): p. 203-218.
8. Roux, E., et al., *Evaluation of the global optimisation method within the upper limb kinematics analysis.* J Biomech, 2002. **35**(9): p. 1279-1283.
9. Herda, L., et al., *Using skeleton-based tracking to increase the reliability of optical motion capture.* Hum Mov Sci, 2001. **20**(3): p. 313-341.
10. Fohanno, V., et al., *Estimating joint kinematics of a whole body chain model with closed-loop constraints.* Multibody System Dynamics, 2014. **31**(4) : p. 433-449.
11. Hill, A.M., et al., *Qualitative and quantitative descriptions of glenohumeral motion.* Gait Posture, 2008. **27**(2): p. 177-88.
12. Tondu, B., *Estimating shoulder-complex mobility*. Applied Bionics and Biomechanics, 2007. **4**(1): p. 19-29.
13. Yang, J., et al., *Review of biomechanical models for human shoulder complex.* International Journal of Human Factors Modelling and Simulation, 2010. **1**(3): p. 271-293.
14. Ackerman, M.J., *The Visible Human Project.* J Biocommun, 1991. **18**(2): p. 14.
15. Duprey, S., L. Cheze, and R. Dumas, *Influence of joint constraints on lower limb kinematics estimation from skin markers using global optimization.* J Biomech, 2010. **43**(14): p. 2858-2862.
16. McClure, P.W., et al., *Direct 3-dimensional measurement of scapular kinematics during dynamic movements in vivo.* J Shoulder Elbow Surg, 2001. **10**(3): p. 269-77.
17. Prinold, J.A.I., A.F. Shaheen, and A.M.J. Bull, *Skin-fixed scapula trackers: A comparison of two dynamic methods across a range of calibration positions.* Journal of Biomechanics, 2011. **44**(10): p. 2004-2007.
18. Warner, M.B., P.H. Chappell, and M.J. Stokes, *Measuring scapular kinematics during arm lowering using the acromion marker cluster.* Human Movement Science, 2012. **31**(2): p. 386-396.
19. McQuade, K.J. and G.L. Smidt, *Dynamic scapulohumeral rhythm: the effects of external resistance during elevation of the arm in the scapular plane.* J Orthop Sports Phys Ther, 1998. **27**(2): p. 125-33.
20. van Andel, C., et al., *Recording scapular motion using an acromion marker cluster.* Gait & Posture, 2009. **29**(1): p. 123-128.
21. Brochard, S., M. Lempereur, and O. Remy-Neris, *Accuracy and reliability of three methods of recording scapular motion using reflective skin markers.* Proc Inst Mech Eng H, 2011. **225**(1): p. 100-5.

22. Senk, M. and L. Cheze, *A new method for motion capture of the scapula using an optoelectronic tracking device: a feasibility study.* Comput Methods Biomech Biomed Engin, 2010. **13**(3): p. 397-401.
23. Horn, B.K.P., *Closed-form solution of absolute orientation using unit quaternions.* Journal of the Optical Society of America A, 1987. **4**(4): p. 629-642.
24. Garner, B.A. and M.G. Pandy, *A Kinematic Model of the Upper Limb Based on the Visible Human Project (VHP) Image Dataset.* Comput Methods Biomech Biomed Engin, 1999. **2**(2): p. 107-124.
25. Dumas, R. and L. Cheze, *Soft tissue artifact compensation by linear 3D interpolation and approximation methods.* J Biomech, 2009. **42**(13): p. 2214-7.
26. Sommer, H.J., 3rd, N.R. Miller, and G.J. Pijanowski, *Three-dimensional osteometric scaling and normative modelling of skeletal segments.* J Biomech, 1982. **15**(3): p. 171-80.
27. Dumas, R. and L. Cheze, *3D inverse dynamics in non-orthonormal segment coordinate system.* Med Biol Eng Comput, 2007. **45**(3): p. 315-22.
28. Garcia de Jalon, J., J. Unda, and A. Avello, *Natural coordinates for the computer analysis of multibody systems.* Comput Methods Appl Mech Eng, 1986. **56**(3): p. 309-327.
29. Salvia, P., et al., *Precision of shoulder anatomical landmark calibration by two approaches: A CAST-like protocol and a new anatomical palpator method.* Gait & Posture, 2009. **29**(4): p. 587-591.
30. Cappozzo, A., et al., *Position and orientation in space of bones during movement: anatomical frame definition and determination.* Clinical Biomechanics, 1995. **10**(4): p. 171-178.
31. Šenk, M. and L. Chèze, *Rotation sequence as an important factor in shoulder kinematics.* Clinical biomechanics (Bristol, Avon), 2006. **21**: p. S3-S8.
32. Dumas, R., et al., *Joint and segment coordinate systems revisited.* Comput Methods Biomech Biomed Engin, 2012. **15 Suppl 1**: p. 183-5.
33. Quental, C., et al., *A multibody biomechanical model of the upper limb including the shoulder girdle.* Multibody System Dynamics, 2012. **28**(1-2): p. 83-108.
34. van der Helm, F.C.T., *A finite element musculoskeletal model of the shoulder mechanism.* J Biomech, 1994. **27**(5): p. 551-569.
35. Bourne, D.A., et al., *Three-dimensional rotation of the scapula during functional movements: an in vivo study in healthy volunteers.* J Shoulder Elbow Surg, 2007. **16**(2): p. 150-62.
36. Chu, Y., et al., *Validation of a video-based motion analysis technique in 3-D dynamic scapular kinematic measurements.* J Biomech, 2012. **45**(14): p. 2462-2466.
37. Massimini, D.F., et al., *In-vivo glenohumeral translation and ligament elongation during abduction and abduction with internal and external rotation.* J Orthop Surg Res, 2012. **7**: p. 29.
38. Nishinaka, N., et al., *Determination of in vivo glenohumeral translation using fluoroscopy and shape-matching techniques.* Journal of Shoulder and Elbow Surgery, 2008. **17**(2): p. 319-322.
39. Ludewig, P.M., et al., *Motion of the shoulder complex during multiplanar humeral elevation.* J Bone Joint Surg Am, 2009. **91**(2): p. 378-89.
40. Anglin, C. and U.P. Wyss, *Review of arm motion analyses.* Proc Inst Mech Eng H, 2000. **214**(5): p. 541-55.
41. van der Helm, F.C. *A standardized protocol for motion recordings of the shoulder*. in *First conference of the international shoulder group*. 1997.
42. Sholukha, V., et al., *Model-based approach for human kinematics reconstruction from markerless and marker-based motion analysis systems.* Journal of Biomechanics, 2013. **46**(14): p. 2363-2371.
43. El Habachi, A., et al., *Global sensitivity analysis of the kinematics obtained with a multi-body optimisation using a parallel mechanism of the shoulder.* Computer Methods in Biomechanics and Biomedical Engineering, 2013. **16**(sup1): p. 61-62.
44. Bourne, D., et al., *Accuracy of digitization of bony landmarks for measuring change in scapular attitude.* Proc Inst Mech Eng H, 2009. **223**(3): p. 349-61.

Appendix

The geometrical data of [24] have been completed using the original VHP data. Table 2 itemises the position of the anatomical landmarks in the thorax SCS [1]. The glenoid cavity (GC) and the humeral head (HH) radii were 32.1 mm and 30.8 mm, respectively. The ellipsoid radii were 104.3 mm, 217.1 mm and 84.1 mm about the X-axis, Y-axis and Z-axis respectively (according to ISB recommendation [1]),. The rotation matrix **C** from the thorax SCS to the ellipsoid coordinate system was:

$$\mathbf{C} = \begin{bmatrix} 0.9494 & -0.0800 & 0.3037 \\ 0.0784 & 0.9968 & 0.0174 \\ -0.3041 & 0.0073 & 0.9526 \end{bmatrix}$$

Table A1: Anatomical landmarks from the VHP (in mm).

	Internal (i.e., bony landmarks)			**External (i.e., skin landmarks)**		
VHP dataset	**X-axis**	**Y-axis**	**Z-axis**	**X-axis**	**Y-axis**	**Z-axis**
IJ	-36.5	7.7	2.9	0	0	0
SC	-37.8	3.9	33.8	-7.2	48.4	31.4
C7	-140.3	80.5	-2.5	-177.8	105.3	0
PX	33.0	-198.7	-7.2	34.1	-198.7	-6.1
AI	-199.4	-72.3	113.0	-224.4	-76.8	131.9
TS	-180.7	47.0	88.5	-204.3	66.6	87.5
AA	-119.8	66.1	199.7	-147.3	73.8	197.4
T8	-203.5	-138.6	0.3	-235.5	-122.1	3.6
AC	-76.5	71.2	180.4	-71.9	84.0	182.4
GH	-88.4	31.9	189.7	*	*	*
HH	-87.7	28.8	190.2	*	*	*
Data from [14] transformed in the thorax segment coordinate system						
IM	-180.5	-75.0	101.7	*	*	*
SM	-153.1	29.0	75.9	*	*	*
EC	-86.8	-160.6	60.9	*	*	*

Figure and table captions

Figure 1a: Subject in static posture with surfaces sensors on the humerus, scapula and thorax

Figure 1b: Physiotherapist performing scapula palpation

Figure 2a: External (•), corresponding internal (--♦), and internal only (♦) anatomical landmarks. The external anatomical landmarks of thorax and scapula (i.e., C7, IJ, T8, PX, AA, AC, TS, and AI) are used to transform the VHP geometry by affine approximation and to obtain the internal anatomical landmarks (i.e., corresponding AA, AC, TS, AI, and SC, SM, IM, EC, HH, GC).

Figure 2b: Parameters $\mathbf{Q}_i = \begin{bmatrix} \mathbf{u}_i \\ \mathbf{r}_{P_i} \\ \mathbf{r}_{D_i} \\ \mathbf{w}_i \end{bmatrix}$ for the humerus, scapula, and thorax segments (i = 1, 2, and 3, respectively, all vectors expressed in an inertial coordinate system, ICS) and schematic representation of the glenohumeral, clavicle (i.e., sternoclavicular and acromioclavicular) and scapulothoracic kinematic constraints (*GH*, *C* and *ST,* respectively).

Figure 3: Scapulothoracic joint angles - Acromial method (blue), multi-body optimisation (red) and palpation method (black) (t-test: NS: non-significant, *: *p-value*<0.05, **: *p-value*<10^{-2})

Table 1: RMSE mean and standard-deviation of all the subjects for each scapulothoracic joint angle

Figure 1

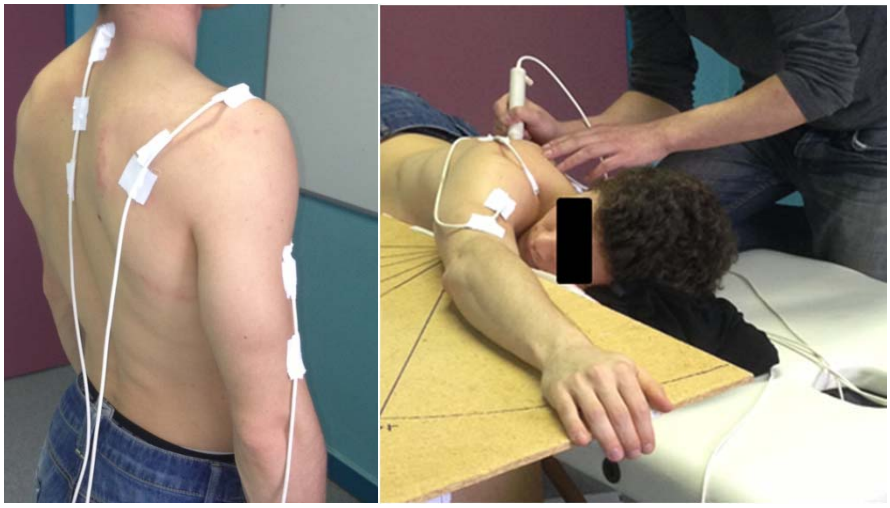

a) **b)**

Figure 2

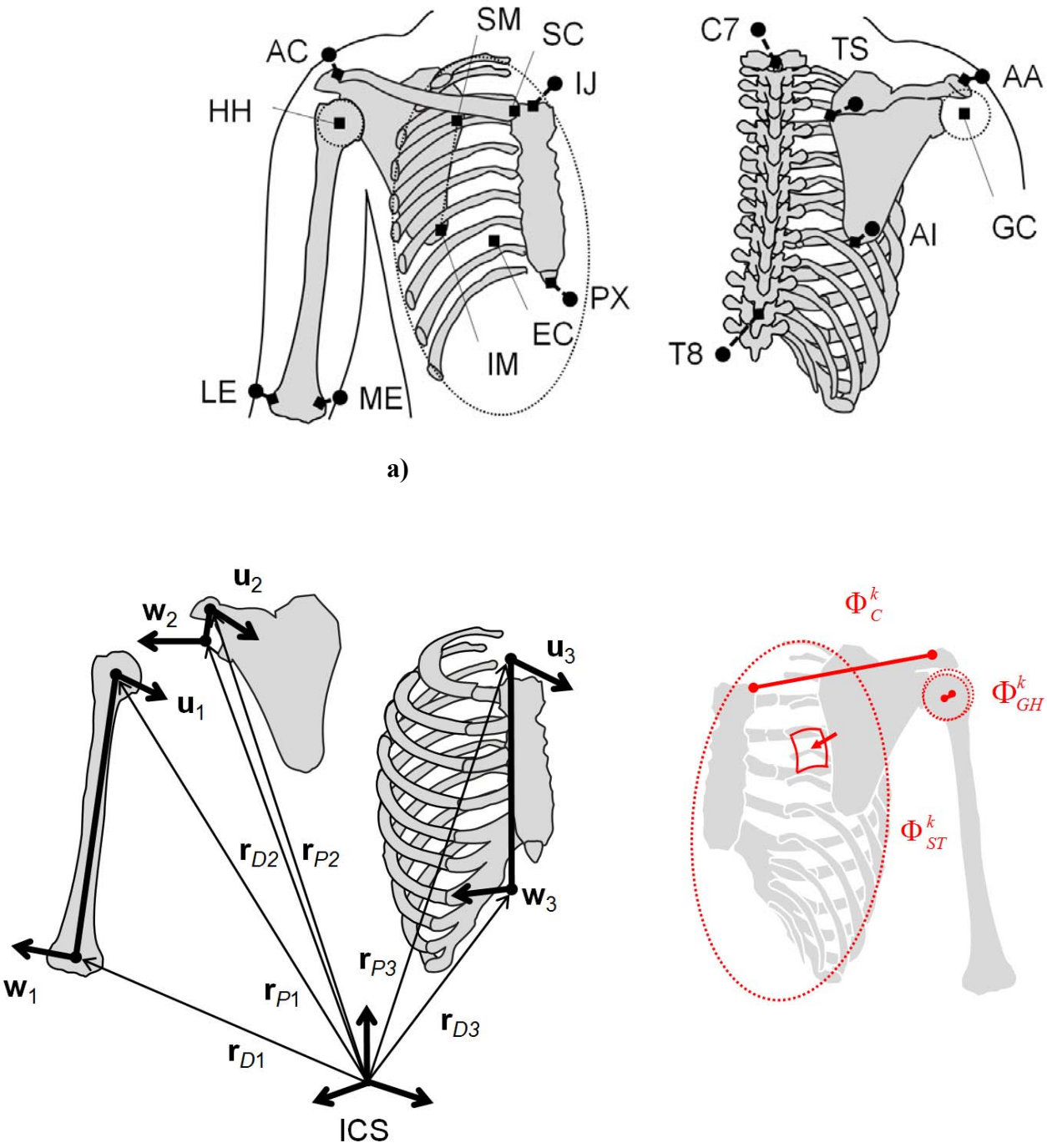
SM
SC
AC
IJ
HH
PX
EC
IM
LE
ME
C7
TS
AA
AI
GC
T8
a)
u2
w2
u1
u3
w3
rD2
rP2
rP3
w1
rP1
rD3
rD1
ICS
b)

Table 1

Scapulo-thoracic joint angles	Internal / External rotation		Downward / Upward rotation		Posterior / Anterior tilt	
	Acromial method	Multi-body optimisation	Acromial method	Multi-body optimisation	Acromial method	Multi-body optimisation
RMSE (in °)	5.80±4.73	9.54±5.66	6.06±4.47	5.72±3.2	6.79 ±4.13	5.29±3.16

Figure 3

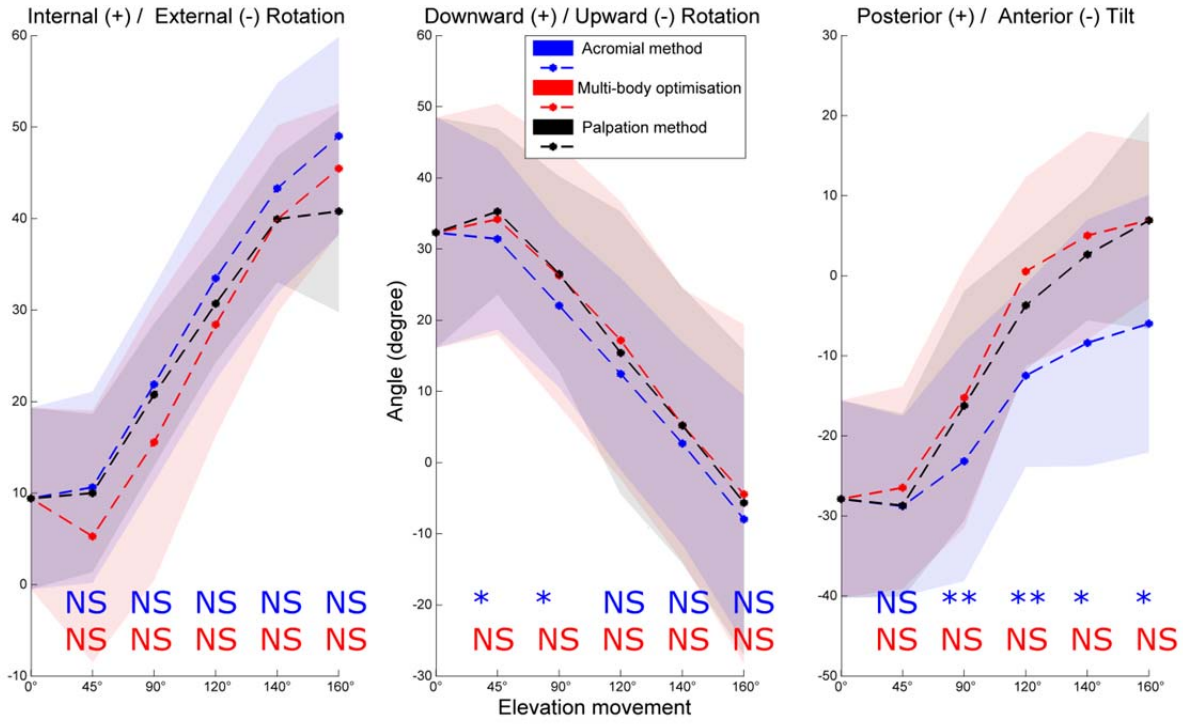
Internal (+) / External (-) Rotation
Downward (+) / Upward (-) Rotation
Posterior (+) / Anterior (-) Tilt
Acromial method
Multi-body optimisation
Palpation method
Angle (degree)
Elevation movement
NS NS NS NS NS
NS NS NS NS NS
* * NS NS NS
NS NS NS NS NS
NS ** ** * *
NS NS NS NS NS